The Three-dimensional Structure of Plasminostreptin, a Bacterial Protein Protease Inhibitor, at 2.8Å Resolution

Nobuo KAMIYA, Masaaki MATSUSHIMA,*,† and Hiromu SUGINO††

Department of Chemistry, Faculty of Science, Nagoya University, Chikusa-ku, Nagoya, Aichi 464

†*Department of Anatomy, Osaka Medical College, Takatsuki, Osaka 569*

††*Central Research Division, Takeda Chemical Industries, Ltd., Jusohonmachi, Yodogawa-ku, Osaka 532*

(Received March 8, 1984)

The three-dimensional structure of plasminostreptin, a bacterial protein protease inhibitor from *Streptomyces antifibrinolyticus*, was determined at 2.8Å resolution by the multiple isomorphous replacement technique. A dimer with the molecular weight of 11,402×2 was included in an asymmetric unit of the crystal. The monomer, composed of 109 amino acid residues, consisted of an antiparallel twisted β-sheet with five strands, two short helices, and irregular polypeptide-chain segments. The reactive site of plasminostreptin belonged to one of these irregular polypeptide-chain segments. The two monomers in the dimer were related by a non-crystallographic pseudo-two-fold axis, and the two β-sheets were arranged face-to-face with each other. The averaged angle between the strands of the two β-sheets was approximately 30° clockwise. In spite of 37 amino acid substitutions including the reactive site residues, the tertiary and quaternary structures of plasminostreptin were similar to those of *Streptomyces* subtilisin inhibitor (SSI). The main-chain conformations of the reactive site of plasminostreptin were similar to those of SSI and other protease inhibitors analysed previously. Moreover, the conformations of the side chain of the evolutionarily conservative asparagine in the so-called "secondary contact region" resembled those found in the inhibitors of the pancreatic secretory trypsin inhibitor family.

Plasminostreptin is a bacterial protein protease inhibitor, isolated from a culture fluid of *Streptomyces antifibrinolyticus* IFO** 13298; it was crystallized by Kakinuma *et al.*[1] It inhibits the proteolytic activities of plasmin, trypsin, and several microbial alkaline proteases (for example, subtilisin) by forming enzyme-inhibitor complexes with the inhibition constants of approximately 10^{-8}M (1M=1 mol dm^{-3}).[1] Two identical monomers are dimerized in a solution. The sequence of 109 amino acid residues comprising the monomer was determined by Sugino *et al.*[2] (Fig. 1), and the molecular weight of the monomer was calculated to be 11,402. The scissile peptide bond of the reactive site was located at Lys69-Gln70.[3] On the basis of the fact that 66% of the amino acid residues, and also the disulfide bonds, are identical with those of *Streptomyces* subtilisin inhibitor (SSI***),[4] plasminostreptin was classified in the SSI family of protein protease inhibitors by Laskowski and Kato.[5] However, the inhibition spectra of plasminostreptin are markedly different from those of SSI.[1,6] Compared with SSI, a total of 37 out of 109 amino acid residues are substituted in plasminostreptin, and Mitsui *et al.*[7] pointed out that some of these residues were inside the SSI molecule. From the preliminary X-ray work for the crystal of plasminostreptin, two monomers were expected in an asymmetric unit. In the case of SSI, however, only one monomer is included in the asymmetric unit. The crystallographic studies of plasminostreptin might reveal the similarities and differences between the structures of plasminostreptin and SSI.

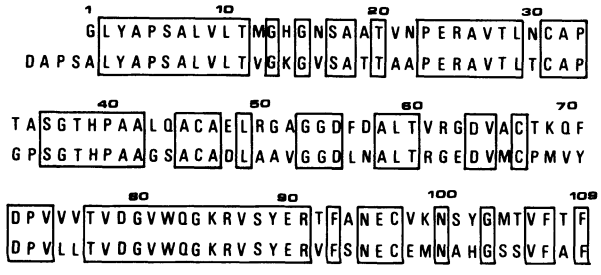

Fig. 1. The amino acid sequences of plasminostreptin[2] and SSI.[4] The residues enclosed by squares are identical between plasminostreptin (1) and SSI (2). To get the sequence number of SSI, four should be added to the number shown here. The scissile peptide bond of plasminostreptin is between Lys69 and Gln70.

The three-dimensional structures of the proteinaceous inhibitors of serine proteases have been studied about the bovine pancreatic trypsin inhibitor [Kunitz] (BPTI),[8] the complex of trypsin with BPTI,[9] and that of trypsin with the soybean trypsin inhibitor [Kunitz] (STI).[10] In addition, the structures of SSI and its complex with subtilisin BPN′ have been determined.[7,11] Recently, three inhibitors of the pancreatic secretory trypsin inhibitor [Kazal] (PSTI) family have also been analysed. These are the third domain of the Japanese quail ovomucoid inhibitor (OMJPQ3),[12] the third domain of the ovomucoid inhibitor from turkey (OMTKY3) complexed with *Streptomyces griseus* protease B,[13] and PSTI complexed with trypsin.[14] In this paper, we wish to report the three-dimensional structure of plasminostreptin at 2.8 Å resolution and to compare it with those of SSI and other inhibitors previously analysed.

Experimental

The Crystals of Plasminostreptin. Plasminostreptin was purified by the method of Kakinuma *et al.*[1] The elongated octahedral crystals of plasminostreptin were prepared at 4 °C in a solution in the absence of any buffer reagent. The typical dimensions of the crystals were 0.6×1.0×1.2 mm^3. The preliminary X-ray photographs revealed that the crystals belonged to the orthorhombic

††Present address: Department of Biochemistry and Molecular Biology, University of Texas, Houston, Texas 77030, U.S.A.

** Institute for Fermentation, Osaka, Japan.

*** Hereafter, the abbreviations for the proteins will be shown in parentheses on their first appearances.

TABLE 1. THE DATA SETS OF THE CRYSTALS OF PLASMINOSTREPTIN

Crystal	Condition	Resolution	Number of reflections	R_M
Native	Non-buffered	2.0Å	14,964(2σ)	0.040
	Phosphate-buffered	2.8Å	6,102(3σ)	0.024
Heavy-atom	0.5 mM $K_2[PtCl_4]$ for 7 days	2.8Å	6,000(3σ)	0.031
Derivatives	1.0 mM $HgBr_2$(2KBr) for 7 days	2.8Å	5,988(3σ)	0.033
	5.0 mM $K[Au(CN)_2]$ for 7 days	2.8Å	5,542(3σ)	0.023

There are two kinds of native crystals. One of them, non-buffered, was grown by the method of Kakinuma *et al.*[1], while the other, phosphate-buffered, was transferred into the phosphate-buffer solution for the MIR technique. The three heavy-atom derivatives were soaked in phosphate-buffer solutions containing the heavy-atom compounds. The reflections whose intensities were more than the values in parentheses (σ was the standard deviation of the reflection intensity) were taken into account in this analysis. The merging R factor, R_M, is defined as follows: $R_M=\sum||F^+|-|F^-||/\sum||F^+|+|F^-||$, where $|F^+|$ and $|F^-|$ are the amplitudes of a Friedel pair.

TABLE 2. THE HEAVY-ATOM PARAMETERS

Derivative	Atom	Occupancy	x	y	z	B
$K_2[PtCl_4]$	Pt1	32 e	0.0204	−0.0145	0.1349	23 Å^2
	Pt2	26	−0.0149	0.2392	0.2540	27
$HgBr_2$	Hg1	26	0.0546	−0.0232	0.1293	31
	Hg2	18	−0.0166	0.2492	0.2690	41
$K[Au(CN)_2]$	Au1	19	−0.0598	0.1606	0.2316	19
	Au2	11	0.0639	0.1493	0.2486	8

The occupancies are converted to the electron unit by using the absolute scale factor, which was calculated through a Wilson plot.[21] (x, y, z) are the fractional coordinates of the atom. The isotropic temperature factors, B, of the Pt and Hg atoms are calculated from the anisotropic temperature factors.

system and that the space group was $P2_12_12_1$. The unit cell dimensions were a=56.88 Å, b=88.87 Å, and c=46.40 Å. Two monomers were expected in an asymmetric unit, which would give the packing density[15] of 2.6 Å^{3}u^{-1}. The crystals were transferred into a phosphate buffer (1.0 M, pH 6.8) for the structure determination by means of the multiple isomorphous replacement (MIR) technique[16] at 2.8 Å resolution. These crystals were regarded as the native crystals. Some of them were soaked in phosphate buffer solutions containing heavy-atom compounds at room temperature. The three heavy-atom derivatives listed in Table 1 were useful in this structure determination.

Data Collection. The X-ray diffraction intensities, including their Friedel pairs, were measured by the use of a computer-controlled four-circle diffractometer, Rigaku AFC-V, set on a rotating anode X-ray generator, Rigaku RU-200. The focus size on the anode was 0.3×3.0 mm^2, and the take-off angle was 6°. The incident X-ray beam was Cu$K\alpha$ radiation monochromatized with a graphite plate, and it was passed through a collimator with the diameter of 0.3 or 0.5 mm. The distance from the crystal to the receiving aperture (3×3 mm^2) was 40 cm. An evacuated beam tunnel was used to avoid X-ray absorption by the air. One of the computer programs for the data collection was modified by Associate Prof. Kyoyu Sasaki of Nagoya University to allow for ordinate analysis.[17] The continuous ω-scan was carried out at a scan speed of 0.04 degree s^{-1} over an angle of 0.72°. The counting time for each reflection was divided into 18 steps. In the ordinate analysis, the extreme three steps on both sides of the scan were regarded as the background, and the remaining twelve steps, as the reflected X-ray peak. In order to monitor the X-ray damage to the crystals, the intensities of four standard reflections were measured every 200 reflection measurements; the damages remained less than 10%. Two crystals were consumed for the data collection of each of the native and heavy-atom derivatives in the MIR technique. Another set of 2.0 Å -resolution data were collected with five original non-buffered crystals and used for the systematic checking of the molecular models.

The Structure Determination. Lorentz-polarization factors, the X-ray-absorption[18] factor, and the damage factor upon X-ray exposure were applied to each of the data sets. The scales between the two or five crystals were calculated using the intensities of the overlapped reflections. The intensity data are summerized in Table 1. After the Kraut scaling,[19] the difference Patterson maps of the derivatives were computed with the coefficients of $(|F_{PH}|-|F_P|)^2$.**** The coordinates of the heavy-atom sites were estimated from these maps. The parameters of these heavy atoms were refined by the phase-refinement procedure[20] (Table 2). The anomalous terms of the heavy atoms contributed only to the inner reflections. The handedness of the heavy-atom parameters were consistent with the calculation of the negative correlation coefficients[22] between the observed and calculated anomalous differences. The refined parameters were used for the calculation of the MIR phases.[23] The averaged figure of merit was 0.61 for the 6,102 reflections. The statistics for the phasing are shown in Table 3.

The MIR electron-density map was calculated at 2.8 Å resolution. The preliminary models of the two independent monomers in an asymmetric unit were built according to the Diamond procedure.[24] The corresponding C$^\alpha$ atoms of each monomer were superposed,[25] and the two monomers could be related by a linear transformation. In order to reduce possible errors in the MIR electron-density map, the electron densities of the two independent monomers were averaged according to the following procedures. (1) Summations of the squared differences between the electron densities at the grid points in one monomer and those at the corresponding points in the other monomer were calculated around the translational vector elements and the angular values estimated from the rotational matrix. (2) Based on the matrix and vector which gave the minimum value of the summation, the MIR electron densities of the two monomers could be averaged. Into this

**** F_{PH} and F_P are structure factors of the heavy-atom derivatives and the native crystal in the MIR technique respectively.

TABLE 3. STATISTICS IN THE MIR PHASING AT 2.8Å RESOLUTION

Crystal	Rc	Rk	Range($4\sin^2\theta/\lambda^2$)	0.016	0.032	0.048	0.064	0.080	0.096	0.112	0.128
Native			$\langle\|F_P\|\rangle$	635	469	516	509	416	328	262	223
			⟨f.o.m.⟩	0.54	0.76	0.70	0.65	0.60	0.59	0.55	0.52
$K_2[PtCl_4]$	0.55	0.109	R_F	0.34	0.20	0.13	0.13	0.13	0.14	0.16	0.16
Derivative			$\langle\|f_H\|\rangle$	80	77	69	62	54	48	44	39
			RMS E	173	66	49	48	43	35	32	30
$HgBr_2$	0.57	0.077	R_F	0.24	0.15	0.09	0.08	0.08	0.09	0.11	0.12
Derivative			$\langle\|f_H\|\rangle$	63	55	47	41	34	30	25	23
			RMS E	86	41	33	31	30	27	24	22
$K[Au(CN)_2]$	0.51	0.087	R_F	0.13	0.09	0.10	0.10	0.10	0.11	0.12	0.15
Derivative			$\langle\|f_H\|\rangle$	48	46	42	36	33	32	30	26
			RMS E	68	34	40	41	34	32	28	30

A total of 6,102 reflection data was divided into eight shells by the range of $4\sin^2\theta/\lambda^2$. The definitions are as follows:
$\langle|F_P|\rangle$; the averaged observed reflection amplitude of the native crystal. ⟨f.o.m⟩; the averaged figure of merit. R_F; $\sum||F_{PH}|-|F_P||/\sum|F_P|$. $\langle|f_H|\rangle$; the averaged calculated structure factor amplitudes of the heavy atoms in the derivative. Rc; $\sum||F_{PH}-F_P|-|f_H||/\sum|F_{PH}-F_P|$ for the centric data. Rk; $\sum||F_{PH}|-|F_P+f_H||/\sum|F_{PH}|$ for all of the reflections whose f.o.m. values are more than 0.85. RMS E; $\{\sum(|F_{PH}|-|F_P+f_H|)^2/n\}^{1/2}$ where n is the number of reflections.

averaged electron-density distribution, a Nicholson model (on a scale of 1 cm/ Å) of one monomer was fitted by using the half-mirror device of Richards.[26] A set of the atomic coordinates was measured on this device. The coordinates for the other monomer in the asymmetric unit were calculated with the linear transformation obtained by the procedure mentioned above. For the systematic checking of the atomic coordinate sets thus obtained, "removed maps"[27] ($|F_o|\exp^{i\alpha c}$) were calculated. The structure factor amplitudes ($|F_o|$) used were the observed 2.0 Å data, and the phases (αc) were those of the structure factors calculated from the atomic-coordinate sets where some atoms were systematically subtracted from the total atoms of the two independent monomers. Some parts of the models were fitted into the electron-density distributions of the "removed maps." The corrected atomic coordinates were refined energetically,[28] and the molecular models were more accurately adjusted to the electron-density distribution according to the Diamond real-space refinement procedure.[29] We believe that the resolution of this structure determination should be regarded as 2.8 Å, since the refinement of the structure with the 2.0 Å resolution data has not yet been completed. Hereafter we will describe the structure of plasminostreptin based on the corrected models.

Results and Discussion

The Monomer Structure. Figure 2 is a schematic illustration of the main chain of the plasminostreptin monomer. The monomer is composed of an antiparallel twisted β-pleated sheet with five strands and two short helices. The five strands of the β-sheet are those of Pro5–Gly15, Arg25–Cys31, Ser36–Thr38, Pro73–Gln83, and Lys85–Phe93. The two helices are defined as the α_1-helix (Ala42–Gly53) and the α_2-helix (Asn95–Gly103), like those of SSI.[7] These helices in the same side of the β-sheet are almost parallel to the sheet and are nearly perpendicular to each other. These secondary structural units are connected by the two disulfide bonds and irregular polypeptide-chain segments. One of the disulfide bonds (Cys31–Cys46) links the α_1-helix to the β-sheet, and the other (Cys67–Cys97) links a part of one of the irregular polypeptide-chain segments to the α_2-helix. The irregular polypeptide-chain segments are in the regions of the N-terminus (Gly1–Ala4), two loops (Asn16–Glu24, Gly54–Asp72), and the C-terminus (Gly103–Phe109). All these regions exist on the surface of the monomer, except for the C-terminal region, which is a part of the hydrophobic core of the monomer. One of the loops (Asn16–Glu24) protrudes from the β-sheet to the interspace between the monomers of the dimer structure (see the following section). The reactive site (Cys67–Phe71) belongs to the other loop (Gly54–Asp72). The site is proximate to the β-sheet and is linked to the α_2-helix by the disulfide bond (Cys67–Cys97). The four residues of Cys31–Thr34 constitute a β-turn, and Pro33 in this turn is in the *cis*-form.[30]

The Dimer Structure. The non-crystallographic relationship between the two monomers in the asymmetric unit is determined by the superposing procedure[25] of the corrected coordinates of the corresponding C^α atoms of each monomer. The rotational matrix and translational vector which relate the two monomers are listed in Table 4. Hereafter, the two monomers will be denoted as the I and II monomers. The centers of gravity calculated from the coordinates of the C^α atoms in angstrom units are (42.2 Å, 25.6 Å, 14.2 Å) and (31.5 Å, 42.4 Å, 25.9 Å) for the I and II monomers respectively. The spherical polar coordinates[31] of the

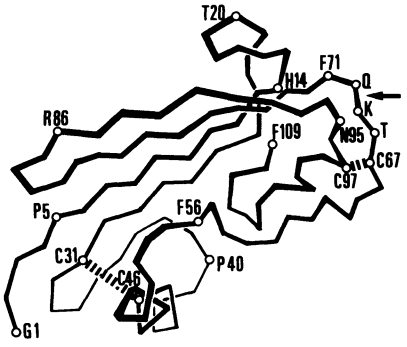

Fig. 2. A schematic drawing of the main chain of the monomer of plasminostreptin. The C^α atoms of 109 amino acid residues are at the creases, and the important positions are identified by open circles together with one letter codes of amino acid residues followed by the sequence number. The arrow represents the scissile peptide bond. The marks (IIIIII) denote the disulfide bonds.

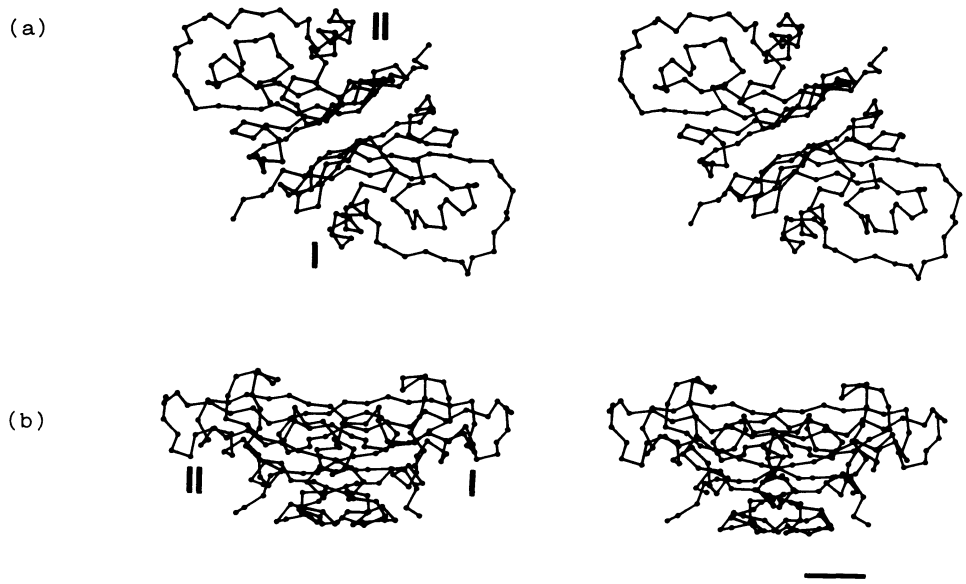

Fig. 3. Stereographic drawings of the plasminostreptin dimer.
The dimer is viewed parallel (a) and perpendicular (b) to the non-crystallographic pseudo-two-fold axis. The models are drawn with the C^{α} atoms. In (a), the lower-right model is the I monomer, and the upper-left is the II monomer. The scale bar in the bottom-right represents 10 Å.

TABLE 4. THE ROTATIONAL MATRIX AND THE TRANSLATIONAL VECTOR OF THE NON-CRYSTALLOGRAPHIC RELATIONSHIP BETWEEN THE I AND II MONOMERS

Rotational matrix			Translational vector
−0.038	−0.133	0.990	22.4
−0.079	−0.988	−0.136	73.0
0.996	−0.083	0.027	−14.4

The atomic coordinates (X, Y, Z) of the II monomer in angstrom units are related to those of the I monomer by this rotational matrix and translational vector: $X = 56.88 \times x$, $Y = 88.87 \times y$, and $Z = 46.40 \times z$, where (x, y, z) are the fractional coordinates.

rotation axis, calculated from the rotational matrix, are 83.7° (from the −y-axis of the unit cell in the x-y plane), 44.2° (from the z-axis), and 182.2° (rotational angle around the rotation axis). The root-mean-square (RMS) deviation is 1.4 Å between the superposed C^{α} atoms. Figure 3 shows the stereo-drawings viewed parallel and perpendicular to the rotational axis. It is possible to conclude that the I and II monomers may be related by a pseudo-two-fold symmetry and may form a dimer. The β-sheet of the I monomer is faced to that of the II monomer in the dimer structure. The topology of stacking β-sheets has been studied by several workers.[32–36] Cohen *et al.*[36] have pointed out that the averaged angle between the strands of the two twisted β-sheets (inter-sheet angle) is from 20° to 50° anticlockwise for the fragments of the immunoglobulin, the Bence-Jones protein, human prealbumin, CuZn superoxide dismutase, and Jack-bean concanavalin A, and that the nonpolar side chains are packed in the interspace between the β-sheets. In the dimer structure of plasminostreptin, the inter-sheet angle was about 30° clockwise, as shown in Fig. 3, and the direction of the rotation is opposite from those studied by Cohen *et al.* Figure 4 shows schematically the arrangement of side chains in between the two β-sheets. In the amino

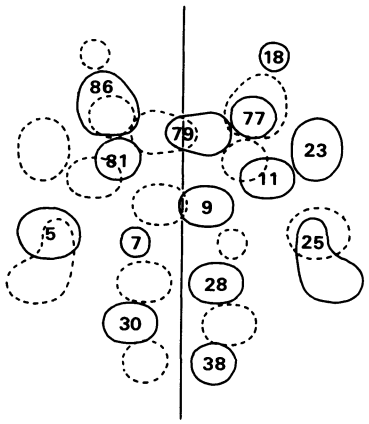

Fig. 4. The arrangement of the side chains between the β-sheets in the dimer. The vertical solid line represents the pseudo-two-fold axis. The side chains which belong to the I monomer are enclosed by the solid lines, and their sequence numbers are given in the circles. The side chains which belong to the II monomer are indicated by the broken circles. The broken circles are related to the solid circles by the pseudo-two-fold symmetry.

acid residues which are in the interspace between the two monomers, the side chains of Pro5, Val9, and Val81 are nonpolar, while those of Asp79 and Arg86 are polar. The side chains of Thr11, Thr28, Asn30, Thr38, and Thr77 are intermediate and can contribute to hydrogen bonds. The Thr11, Thr28, Asn30, Thr38, Thr77, Asp79, and Arg86 of both of the monomers either can be formally charged or can contribute to hydrogen bonds. The side chains of Val9 and Thr28 are close to the pseudo-two-fold axis which related the I and II monomers, and these side chains of the two monomers were in contact with each other. The side chain of Arg86 in one monomer could be expected to interact with the side chains of Thr11, Thr77, and

Asp79 in the other monomer. The side chain of Arg86 would not, however, interact with those of Thr11, Thr77, and Asp79 in an orientation of β-sheets where the inter-sheet angle was 20° to 50° anticlockwise, as in the proteins studied by Cohen *et al.*,[36] but it could interact with them in the orientation of the two monomers of plasminostreptin where the inter-sheet angle was about 30° clockwise.

Comparisons between the Main Chains of Plasminostreptin and SSI. According to the superposing procedure[25] of the corresponding C^{α} atoms, the RMS deviations are 1.4 Å for all the following combinations: the I monomer and the SSI subunit, the II monomer and the SSI subunit, and dimeric plasminostreptin and dimeric SSI. Therefore, the overall structure of plasminostreptin resembles that of SSI not only in the tertiary structure of the monomer, but also in the quaternary structure of the dimer. Compared with the sequence of SSI, a total of 37 out of 109 amino acid residues of plasminostreptin are substituted (see Fig. 1). Eight of these substituted residues are Met12, Val21, Ala52, Phe56, Val75, Val76, Lys99, and Thr108, whose side chains are buried in the monomer. The side chains of the other substituted residues are exposed to the solvent. Mitsui *et al.*[7] expected that the buried side chains could be accommodated in the SSI structure. Their expectations are, in fact, confirmed in the plasminostreptin structure. The residue of Phe56 may be noteworthy in these substitutions, since the total volume of the side chain is considerably larger than that of the corresponding residue, Leu60, of SSI. In the plasminostreptin structure, the benzene moiety of the phenylalanine is packed between the β-sheet and the α_1-helix, and it is nearly parallel to the β-sheet. The torsion angle around the C^{α}–C^{β} bond, χ_1, is similar to that of SSI. This kind of substitution is also found between the structures of the complexes of *Streptomyces griseus* protease A with Ac-Pro-Ala-Pro-Phe-H or -Phe-OH[37] and of *Streptomyces griseus* protease B with OMTKY3.[13] The P_1 residue is substituted from the phenylalanine of the tetrapeptides to the leucine residue in OMTKY3. The side chains are inserted between a β-sheet and a polypeptide chain, and they exist at almost the same position as the specific binding pocket of the enzyme. The substitution only slightly affects the conformations around them. Between the structures of plasminostreptin and SSI, no significant movement of the α_1-helix could be detected. However, the substitution might cause small conformational changes in the side chains around the phenylalanine residue.

Comparisons of the Reactive Site Region with the Inhibitors Already Analysed by X-Ray Crystallography. According to the classification of Laskowski and Kato[5], the six inhibitors which have already been analysed by X-ray crystallography may be classified into four families: the BPTI [Kunitz], STI [Kunitz], PSTI [Kazal], and SSI families. These four families are genetically different, and their main-chain foldings are also different from each other. It is, however, noticeable that the main-chain conformations of the reactive sites (the residues from P3 to P2′[38]) are homologous.[7] Their main-chain torsion angles, phi and psi, are listed in Table 5. The angles of the reactive site of plasminostreptin are similar, in spite of the differences in the amino acid sequences and their inhibitory specificities. These similarities can be expected as examples of convergent evolution.[39] Figure 5 shows the structures around the reactive site regions of plasminostreptin, SSI, and OMJPQ3. The structure of OMJPQ3 can be deemed as representing the inhibitors of the PSTI [Kazal] family, since the three inhibitors, OMJPQ3, OMTKY3, and PSTI, belonging the same inhibitor family turned out to have very similar overall structures.[12–14] The structure around the reactive site of plasminostreptin closely resembles those of SSI and OMJPQ3. (The benzene moiety of Phe71 in plasminostreptin extends to a different direction from those of the phenol moieties of Tyr75 in SSI and Tyr20 in OMJPQ3. This difference may be caused by the crystal packing, because the side chains of Phe71 and Asp72 are in close contact with the residues of Phe71 and Asn16 respectively of a neighboring monomer in the present crystal.) It is interesting to note that an asparagine residue in the secondary contact region[39] is evolutionarily conservative. The residues are Asn95 in plas-

TABLE 5. THE MAIN-CHAIN CONFORMATIONS OF THE REACTIVE SITES OF BPTI,[8] STI,[10] SSI,[a] OMJPQ3,[12] AND PLASMINOSTREPTIN, AND THEIR RESIDUES

	P3		P2		P1		P1′		P2′	
	phi	psi	phi	psi	phi	psi	phi	psi	phi	psi
BPTI	−86°	−7°	−89°	165°	−127°	32°	−77°	178°	−134°	88°
STI	−46	−21	−77	136	−89	85	−135	−115	−175	−179
SSI	−123	144	−55	130	−74	76	−103	170	−117	96
OMJPQ3	−121	153	−64	160	−102	18	−61	138	−105	92
Plasminostreptin (tentative)	−120	168	−78	166	−127	29	−78	133	−95	72

BPTI	Pro	Cys	Lys(15)	Ala	Arg
STI	Ser	Tyr	Arg(63)	Ile	Arg
SSI	Cys	Pro	Met(73)	Val	Tyr
OMJPQ3	Cys	Pro	Lys(18)	Val	Tyr
Plasminostreptin	Cys	Thr	Lys(69)	Gln	Phe

The angles of plasminostreptin are those of the I monomer and should be regarded as tentative, since the structure refinement is not yet finished. a) The angles of SSI are those partially refined with the 2.3Å resolution data (R=27%; private communication from Dr. Yukio Mitsui).

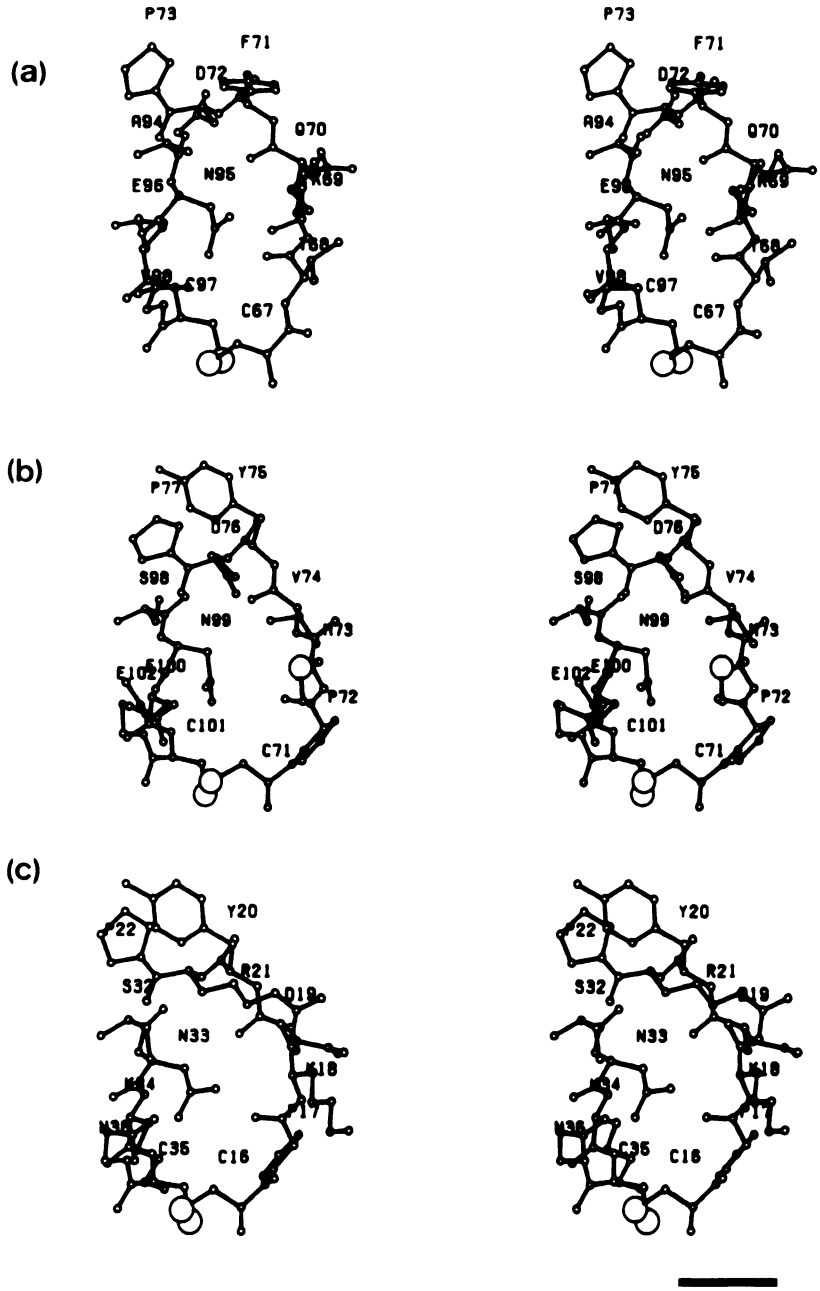

Fig. 5. Similarities of the structures around the reactive sites of plasminostreptin (a), SSI (b), and OMJPQ3 (c).
The reactive site of plasminostreptin is drawn with the coordinate set of the I monomer. The coordinate set of SSI was taken from the Protein Data Bank. The structure of OMJPQ3 is based on the coordinates kindly provided by Prof. Dr. Robert Huber. These structures are viewed from the nearly equivalent direction which was determined by means of the superpositions of the corresponding C^{α} atoms. The large open circles are the sulfur atoms. The residue names are represented by one letter codes followed by the sequence numbers. The scale bar in the bottom-right corner represents 5 Å.

minostreptin, Asn99 in SSI, and Asn33 in OMJPQ3. In all of the three inhibitors of the PSTI [Kazal] family, the side chain of the asparagine residue exists between the reactive site loop and the inner α-helix, connecting them with hydrogen-bonding networks.[12–14] Such a network in the OMJPQ3 structure consists of three hydrogen bonds between the N^{δ} atom of Asn33 and the main-chain carbonyl oxygen atoms of Pro17 and Asp19 in the reactive site, and between the O^{δ} atom of Asn33 and the peptide nitrogen atom of Asn36 in the α-helix.[12] Fujinaga *et al.*[13] considered this network to be essential for the inhibitory mechanism. It resists the formation of the tetrahedral intermediate of the proteolysis at the carbonyl-carbon atom of the scissile peptide bond.

This network has not been found in the SSI structure[7], but it seems likely to exist in the plasminostreptin structure, as shown in Fig. 5. The structure of plasminostreptin is being refined, and the conformations of Asn95 can be defined more precisely after the refinements.

The authors wish to thank Associate Professor Noriyoshi Sakabe, Dr. Kiwako Sakabe, and Associate Professor Kyoyu Sasaki of Nagoya University for their helpful suggestions in studying this structure and their critical advice in the preparation of this manuscript. We are also greatly thankful for the help of Professor Dr. Robert Huber of the Max-Planck-Institut für Biochemie in kindly informing us of the OMJPQ3 and PSTI structures. We also wish to thank Drs. Masao Nishikawa and Atsushi Kakinuma of Takeda Chemical Industries, Ltd., for their support and encouragement throughout this work. One of us (M. M.) is especially grateful to Professor Takashi Kihara of Osaka Medical College for his great encouragement during this study, and one of us (N. K.) is a holder of a scholarship from the Toyoda Physical and Chemical Research Institute. The computations were done at the Nagoya University Computation Center and Computer Center of the Institute for Molecular Science.

References

1) A. Kakinuma, H. Sugino, N. Moriya, and M. Isono, *J. Biol. Chem.*, **253**, 1529 (1978).
2) H. Sugino, A. Kakinuma, and S. Iwanaga, *J. Biol. Chem.*, **253**, 1546 (1978).
3) H. Sugino, S. Nakagawa, and A. Kakinuma, *J. Biol. Chem.*, **253**, 1538 (1978).
4) T. Ikenaka, S. Odani, M. Sakai, Y. Nabeshima, S. Sato, and S. Murao, *J. Biochem.*, **76**, 1191 (1974)
5) M. Laskowski, Jr. and I. Kato, *Annu. Rev. Biochem.*, **49**, 593 (1980).
6) S. Sato and S. Murao, *Agric. Biol. Chem.*, **37**, 1067 (1973).
7) Y. Mitsui, Y. Satow, Y. Watanabe, and Y. Iitaka, *J. Mol. Biol.*, **131**, 697 (1979).
8) J. Deisenhofer and W. Steigemann, *Acta Crystallogr., Sect. B*, **31**, 238 (1975).
9) R. Huber, D. Kukla, W. Bode, P. Schwager, K. Bartels, J. Deisenhofer, and W. Steigemann, *J. Mol. Biol.*, **89**, 73 (1974).
10) R. M. Sweet, H. T. Wright, J. Janin, C. H. Chothia, and D. M. Blow, *Biochemistry*, **13**, 4212 (1974).
11) S. Hirono, K. T. Nakamura, Y. Iitaka, and Y. Mitsui, *J. Mol. Biol.*, **131**, 855 (1979).
12) E. Papamokos, E. Weber, W. Bode, R. Huber, M. W. Empie, I. Kato, and M. Laskowski, Jr., *J. Mol. Biol.*, **158**, 515 (1982).
13) M. Fujinaga, R. J. Read, A. Sielecki, W. Ardelt, M. Laskowski, Jr., and M. N. G. James, *Proc. Natl. Acad. Sci. U. S. A.*, **79**, 4868 (1982).
14) M. Bolognesi, G. Gatti, E. Menegatti, M. Guarneri, M. Marquart, E. Papamokos, and R. Huber, *J. Mol. Biol.*, **162**, 839 (1982).
15) B. W. Matthews, *J. Mol. Biol.*, **33**, 491 (1968).
16) D. Harker, *Acta Crystallogr.*, **9**, 1 (1956).
17) I. J. Tickel, *Acta Crystallogr., Sect. B* **31**, 329 (1975).
18) A. C. T. North, D. C. Phillips, and F. S. Mathews, *Acta Crystallogr., Sect. A*, **24**, 351 (1968).
19) J. Kraut, L. C. Sieker, D. F. High, and S. T. Freer, *Proc. Natl. Acad. Sci. U. S. A.*, **48**, 1417 (1962).
20) H. Müirhead, J. M. Cox, L. Mazzarella, and M. F. Perutz, *J. Mol. Biol.*, **28**, 117 (1967).
21) A. J. C. Wilson, *Acta Crystallogr.*, **2**, 318 (1949)
22) P. M. Colman, J. N. Jasonius, and B. W. Matthews, *J. Mol. Biol.*,**70**, 710 (1972).
23) D. M. Blow and F. H. C. Crick, *Acta Crystallogr.*, **12**, 794 (1956).
24) R. Diamond, *Acta Crystallogr.*, **21**, 253 (1966).
25) K. Nishikawa and T. Ooi, "Program System for Protein Conformation Study II," Report of PSPCS Group for a Grant-in-Aid for Scientific Reseach from Ministry of Education (1978), p. 49.
26) F. M. Richards, *J. Mol. Biol.*, **37**, 225 (1968).
27) M. Vijayan, "Computing in Crystallography," ed by R. Diamond, S. Ramaseshan, and K. Vankatesan, Bangalore, Indian Academy of Sciences for the International Union of Crystallography (1980), 19.01—19.26.
28) M. Levitt, *J. Mol. Biol.*, **82**, 393 (1974).
29) R. Diamond, *Acta Crystallogr., Sect. A*, **27**, 436 (1971).
30) P. N. Lewis, F. A. Momany, and H. A. Scheraga, *Biochem. Biophys. Acta*, **303**, 211 (1973).
31) N. Tanaka, *Acta Crystallogr., Sect. A*, **33**, 191 (1977).
32) M. Levitt and C. Chothia, *Nature (London)*, **261**, 552 (1976).
33) M. J. E. Sternberg and J. M. Thornton, *J. Mol. Biol.*, **110**, 285 (1977).
34) J. S. Richardson, *Nature (London)*, **268**, 495 (1977).
35) C. Chothia, M. Levitt, and D. Richardson, *Proc. Natl. Acad. Sci. U. S. A.*, **74**, 4130 (1977).
36) F. E. Cohen, M. J. E. Sternberg, and W. R. Taylar, *J. Mol. Biol.*, **148**, 253 (1981).
37) M. N. G. James, A. R. Sielecki, G. D. Brayer, L. T. J. Delbaere, and C. A. Bauer, *J. Mol. Biol.*, **144**, 43 (1980).
38) I. Schechter and A. Berger, *Biochem. Biophys. Res. Commun.*, **27**, 157 (1967).
39) Y. Mitsui, Y. Satow, Y. Watanabe, S. Hirono and Y. Iitaka, *Nature (London)*, **277**, 447 (1979).